Tribology International 196 (2024) 109668

Contents lists available at ScienceDirect

Tribology International

journal homepage: www.elsevier.com/locate/triboint

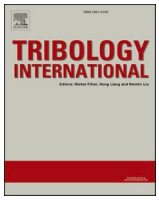

Effects of interface friction states on plastic deformation in metal surface and bulk

Xiaoke Lin, Tatsuya Sugihara *, Toshiyuki Enomoto

Department of Mechanical Engineering, Graduate School of Engineering, Osaka University, 2–1, Yamada-oka, Suita, Osaka 565–0871, Japan

ARTICLE INFO

Keywords:
Interface friction
In-situ observation
Boundary layer
Surface expansion

ABSTRACT

Interface friction at the tool/die-material interface plays a pivotal role in metal plastic processes, significantly impacting material deformation behavior near the contact surface. This study focuses on understanding friction-induced deformation, particularly the plastic boundary layer and surface expansion behavior, at the tool/die-material interface by employing direct in-situ observations, coupled with high-speed imaging and particle image velocimetry techniques. It proves that interface friction determines the wall-slip behaviors and subsequently results in the non-uniform surface expansion distribution. Moreover, our results indicate that the application of lubricant alters the wall-slip velocity and localized surface expansion by 60% and 76%, respectively, at the contact interface. Based on these observations, a quantitative method for assessing the effectiveness of lubrication is proposed.

1. Introduction

Tool/die-material interfaces in metal plastic forming processes are characterized by severe conditions of friction and temperature [1]. These conditions have a pivotal role in bulk deformation, energy consumption and surface quality [2,3]. For example, friction at the tool-workpiece interface plays an important role in determining the strain distributions [4] and non-uniform friction stress can result in uneven strain distribution, leading to the material failure, such as wrinkling or tearing [5]. In addition, friction between the die and workpiece is fundamental to the efficiency and quality of the metal forming process, affecting the formability of bulk material, tool life, as well as the surface finish of the specimen [6,7].

In such severe interface friction conditions, a phenomenon of material flow localization caused by variations in velocity gradients occurs near the tool/die-material contact interface, significantly impacting material removal processes and the quality of material forming [8,9]. It has been reported that this localization of material flow is very similar to fluid-like boundary layer, for which a fluid is forced to flow over a flat plate [10,11], whereas the existence of wall-relative velocity at tool-material interface indicates that traditional no-slip boundary condition may not be well-matched this deformation behavior [12]. The no-slip assumption at the liquid/solid interface, which has been widely supported by extensive experimental evidence in macroscopic analyses of fluid film lubrication [13], contrasts with microscopic scales where localized sliding occurs at the interface [14]. This phenomenon, akin to the slip observed at the tool-material interface, suggests non-uniform friction conditions along the contact surface [12,15]. The presence of flow localization and slip conditions at the tool/die-material interface clearly illustrates the deformation characteristics near the contact interface arising from interface friction. Therefore, it is essential for understanding the fundamental friction phenomena to clarify the relationship between interface friction and deformation behaviors, encompassing boundary layer structures.

For example, one of the characteristic deformation phenomena reflecting the friction condition at the sliding surface is surface expansion of the bulk material. In metal plastic processes, work material undergoes extensive deformation and experiences high surface expansion, characterized by a significant ratio between the incremental surface area of the final product and the original undeformed surface area of the workpiece [16]. This heightened surface expansion exposes chemically active nascent surfaces, leading to pronounced adhesion at the interface [17]. Consequently, understanding the behavior of surface expansion plays a pivotal role in comprehending tribological properties under severe contact conditions. It is also recognized that severe surface expansion caused by plastic deformation of the workpiece results in flattening of the asperities on the contact surface, intensifying frictional traction and significantly altering tribological properties [18]. This often

* Corresponding author.
E-mail address: t-sugihara@mech.eng.osaka-u.ac.jp (T. Sugihara).

https://doi.org/10.1016/j.triboint.2024.109668
Received 29 January 2024; Received in revised form 5 April 2024; Accepted 14 April 2024
Available online 16 April 2024

results in the transfer of workpiece material onto the tool/die, leading to damage on specimen surfaces [19]. Our prior study has investigated the surface expansion behavior of the contact surface and its influence on interfacial adhesion phenomena. As a result, the distribution of surface expansion, unevenly distributed along the sliding surface, closely aligns with that of adhesion force [20]. Although the factors determining the distribution of surface expansion are still under discussion, investigating the development of the boundary layer structure might elucidate the role in how the surface of bulk material expands at the contact interface. This is because both surface expansion and the plastic boundary layer result from interface friction under severe sliding contact conditions.

Although the influence of interface friction on deformation behavior, like boundary layer phenomenon and surface expansion behavior, is widely acknowledged, quantitative discussions on these matters have been limited primarily due to the extreme difficulty in quantitatively investigating deformation behavior at tool/die-material interfaces using traditional methods [21,22]. Recently, particle image velocimetry (PIV) has emerged as a method for studying material flow in severe plastic deformation of metals [23]. This technique has been effectively employed for in-situ observation of plastic flow in metal deformation processes, encompassing cutting and forming [24–26]. This innovation introduces a pioneering approach for directly observing interface phenomena in metal plastic processes. It facilitates the exploration of the quantitative correlation between interface friction and deformation field, thereby advancing our understanding of the influence of interface friction on interface deformation. Such insights enhance our comprehension of tribology applications in fundamental machining or forming processes.

In this study, wedge indentation experiments are conducted as a model system to clarify the severe flow localization at tool/die-material interfaces in metal plastic processes. Direct in-situ observations, coupled with high-speed imaging and particle image velocimetry techniques, are employed to quantify plastic deformation behavior, including surface expansion at the contact interface, and compare it with traditional boundary layer theory. Specifically, the quantitative relationship between interface friction and interface deformation, namely wall-slip phenomenon and surface expansion behavior at the interface, is investigated. Through PIV analysis, the critical factors influencing surface expansion distribution are explored. Moreover, it examines the effects of interface friction on boundary layer phenomena and the distribution of surface expansion, proposing novel quantitative methods for evaluating lubrication effectiveness during indentation processes.

2. Experimental details

2.1. Experimental setup

Aluminum is a typical metallic material with a wide range of applications. Additionally, the aluminum undergoes significant deformation at the interface and exhibits severe adhesion during the indentation process, facilitating the exploration of the interface friction and deformation field relationship [27]. On the other hand, the observed deformation field near the contact interface during wedge indentation exhibits remarkable similarities to those observed in various plastic forming processes, suggesting its applicability across diverse scenarios [12,28]. Hence, in this study, annealed aluminums (A1050P) were employed as the workpiece material and wedge indentation experiments were conducted as a model system to explore the effects of interface friction on metal deformation. Fig. 1 shows the schematic of the experimental setup of direct in-situ observations for the indentation. To observe the plastic flow that occurs inside the material, a plane strain condition was ensured by clamping the specimen against a thick, transparent glass block, which restricts out-of-plane deformation. The specimens were then subjected to indentation at a specific speed (0.1 mm/s) using high-speed steel wedges with apex angles (2α) of 30°. The material flow was recorded in situ using a high-speed camera, capturing

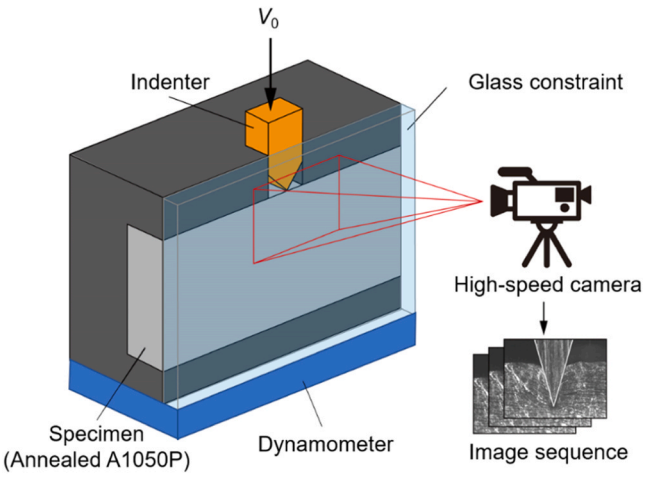

Fig. 1. Schematic of the experimental setup for in-situ observations.

images at 125 frames per second and with a spatial resolution of 1.0 μm per pixel. The image sequences were analyzed by image correlation using particle image velocimetry (PIV) [29].

Throughout this process, the indentation force in the vertical direction was measured using a piezoelectric dynamometer mounted under the material (Fig. 1). Note that the glass block was removed when measuring the indentation force to eliminate the influence of the friction between the glass and indenter. Fig. 2 shows an example of the change in indentation force during experiments at a depth of 1 mm with an indentation speed of 0.1 mm/s and the equilibrium of forces that act on the indenter, respectively. As shown in Fig. 2(a), the force demonstrates a linear increase throughout the indentation process, reaching its peak at a specific indentation depth. After stopping for 1 s, the indenter is extracted from the specimen. Additionally, the maximum force (F) represents the resisting force that impedes the indenter from penetrating and separating the material, resulting from the combined effects of friction force (F_f) and normal force (F_n) (see Fig. 2(b)). Their relationship with the indenter angle can be expressed as:

$$\frac{F}{2} = F_f \cos\alpha + F_n \sin\alpha \tag{1}$$

The friction force at the indenter-material interface acts as the primary resistance force preventing the penetration of the indenter, concurrently causing shear deformation at the contact surface. Due to the symmetrical shape of the indenter, directly measuring the friction force and normal force separately is unfeasible. Given the relatively narrow angle of the indenter used in our experiments ($\alpha = 15^{\circ}$), the normal component of the normal force to the indenter surface is comparatively small compared to the normal component of the friction force. Hence, the maximum indentation force value was employed to assess the magnitude of the friction force in this study.

2.2. Friction distribution along the indenter face

It is expected that the friction stress at the indenter-material interface exhibits non-uniform distribution along the side face of the indenter (indenter face) and the friction condition becomes more severe toward the indenter tip. To verify this hypothesis, indentation experiments were conducted using both normal and micro-grooved indenters to measure the indentation force with the indentation depth of 1 mm. Given that the indentation force, predominantly influenced by the friction force (F_f) and normal force (F_n), is primarily dictated by the former due to the narrow indenter angle, evaluating the maximum indentation force value enables the assessment of the magnitude of the friction force in this study. Fig. 3 shows the observation of a micro-grooved indenter (I-400), and Table 1 summarizes the micro-grooved indenters used in this study.

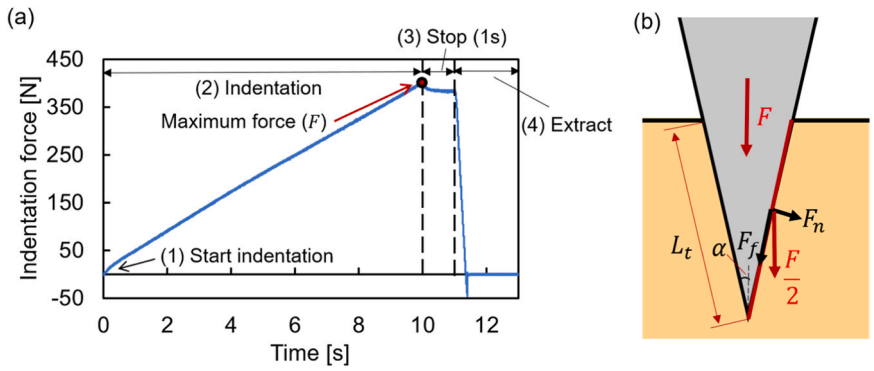

Fig. 2. (a) Procedure for obtaining indentation force and (b) relationship between each force component.

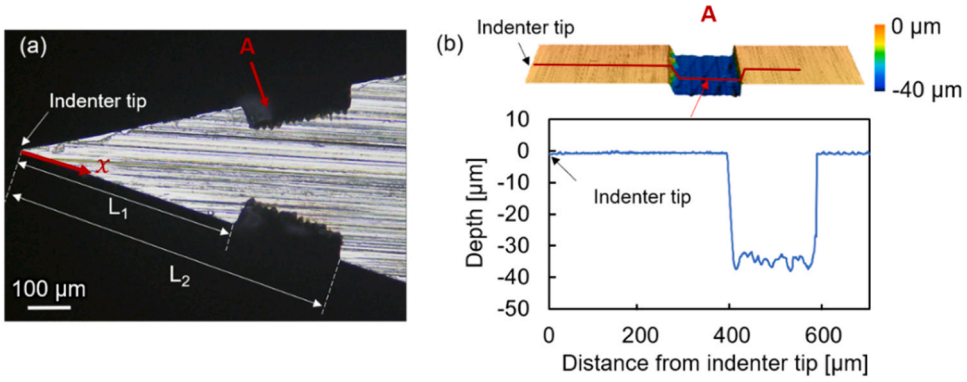

Fig. 3. Observation of single micro-groove (I-400): (a) optical microscope image and (b) 3-D and 2-D profiles.

Table 1
The configurations of the fabricated indenters.

Indenter name	L_1 (μm)	L_2 (μm)	Depth of groove D (μm)	x_m (mm)
I-300	300	500	30	0.4
I-400	400	600	30	0.5
I-500	500	700	30	0.6
I-600	600	800	30	0.7

As shown in Fig. 3, a single micro-groove was fabricated on each side face of the indenter utilizing femto-second laser technology [30].

Assuming that x is the distance along the indenter face from the indenter tip and the stress distributed on the indenter face is $\tau(x)$, the indentation force (F) and the force generated partially within the area between $L_1 < x < L_2$ (F_{12}) when using a normal indenter without micro-grooves can be expressed as:

$$F = 2\int_0^{L_t} w\tau(x)dx \tag{2}$$

$$F_{12} = \int_{L_1}^{L_2} w\tau(x)dx \tag{3}$$

Here, L_t represents the contact length between the indenter face and the specimen (see Fig. 2(b)), and w is the width of the specimen. Fig. 4(a) compares the variation in indentation force over time at an indentation depth of 1 mm with a speed of 0.1 mm/s for both the normal indenter and I-300 grooved indenter. The result demonstrates that, at t = 3.0 s (D = 0.3 mm), which corresponds to the moment the bottom of the micro-groove (L_1) begins contacting the material, the indentation force for I-300 grooved indenter decreases compared to that of the normal indenter, and this trend continues even when the upper edge of the

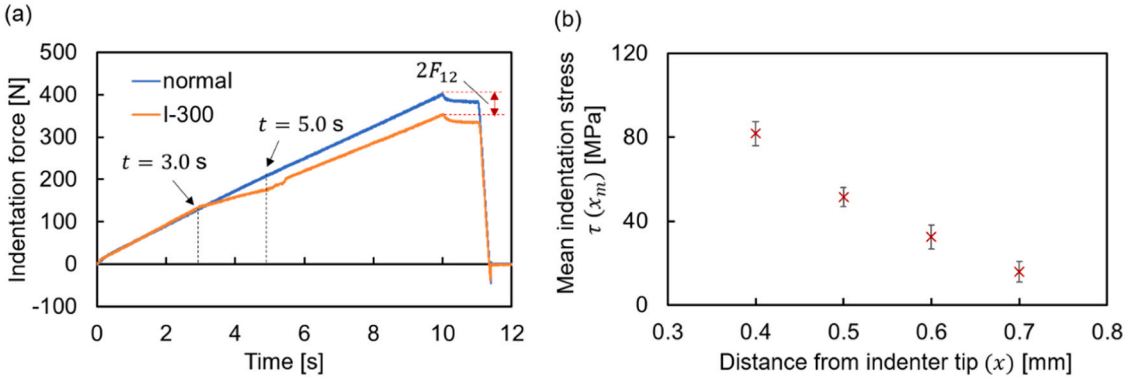

Fig. 4. (a) Indentation force for normal and I-300 grooved indenters, and (b) mean indentation stress distribution along the indenter face.

micro-groove (L_2) starts to make contact with the material at t = 5.0 s. This confirms that the difference in the maximum indentation force between the normal and grooved indenters is attributable to their differing contact conditions. Hence, in the case of the micro-grooved indenter, where the grooved area $L_1 < x < L_2$ is in a non-contact state at the interface, F_{12} becomes 0. Consequently, the indentation force for the grooved indenter F_{groove} can be described as:

$$F_{groove} = F - 2F_{12} \tag{4}$$

Based on this equation, F_{12} can be determined as:

$$F_{12} = \frac{F - F_{groove}}{2} \tag{5}$$

Therefore, the distribution of the partially generated force along the indenter face can be estimated by employing indenters with micro-grooves fabricated at different positions on the side face of the indenter. The mean stress at the middle point of the micro-groove x_m ($x_m = L_1 + (L_2 - L_1)/2$, (see Table 1)) can be calculated using the formula:

$$\tau(x_m) = \frac{F_{12}}{w(L_2 - L_1)} = \frac{F - F_{groove}}{2w(L_2 - L_1)} \tag{6}$$

Fig. 4(b) shows the relationship between the distance from the indenter tip (x) and the stress value at $x = x_m$, i.e., $\tau(x_m)$, obtained by using each micro-grooved indenter. As shown in this figure, the local indentation force, specifically the indentation stress at the material-indenter interface, increases as the distance from the indenter tip decreases. The distribution of mean indentation stress, derived from Eq. 6, closely mirrors that of the frictional shear stress along the interface due to the narrow indenter angle. Therefore, these results clearly verify a linear increase in friction stress along the side face of the indenter towards the indenter tip (Fig. 4(b)). Based on this friction stress distribution, the relationship between interface friction and the plastic deformation behavior in the vicinity of the interface will be further discussed in this paper.

3. Results and discussions

3.1. The influence of the interface friction on the boundary layer phenomenon

Boundary layer phenomena hold significant importance in fluid mechanics, wherein a thin layer of fluid forms over a solid surface due to differences in velocity gradients [31]. It has been reported that the deformation field in the vicinity of severe sliding contact caused the friction induced retardation of material flow, such as tool-chip interface in machining process and die/mold-material interface in forming process, resembles a fluid-like boundary layer flow [10,11]. To understand the relationship between the friction condition and plastic boundary layer structure, wedge indentation experiments were conducted. Fig. 5 shows the deformation field superimposed by the streaklines obtained by the PIV analysis. In Fig. 5(a), the initial streak lines U_n (n: streakline number) at $t = t_0$ are placed orthogonal to the indenter face, i.e., the X and Y axes are tangential and normal to the indenter face, respectively. Fig. 5(b) shows the material flow at $t = t_0 + 5$ s. The yellow and red points in these figures correspond to the endpoints of the streaklines and points on the indenter face tangent to the initial position of the endpoints, respectively. In other words, the gap between red point and yellow point for each streakline at $t = t_0 + 5$ s (Fig. 5(b)) indicates the relative motion between the material and indenter at the interface.

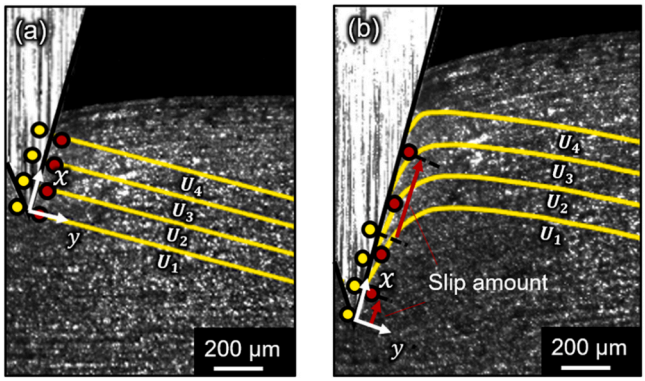

Fig. 5. Material flow at (a) $t = t_0$, (b) $t = t_0 + 5$ s.

The friction at the interface induces a shear stress tangential to the bulk material near the indenter surface, which is transmitted to the workpiece and influences its deformation behavior. As depicted by the streaklines in Fig. 5(b), the material displacement along the x-direction gradually diminishes and eventually becomes stationary at a distance from the indenter face, indicating the existence of velocity gradients of the bulk deformation. This result shows that the material is dragged by the interface friction between the indenter and material, which consequently results in the formation of a plastic boundary layer.

The characteristics of this friction-induced deformation are also evident in the distribution of the velocity in x direction (v_x), i.e., velocity of the material along the indenter face, as shown in Fig. 6. Note that the velocity field is determined by averaging velocities over 20 consecutive frames, and $v_x(x,y)$ denotes the value of v_x at the coordinate (x,y). Fig. 6 (a) confirms that the formation of a steep velocity gradient that constitutes the plastic boundary layer. Also, Fig. 6(b) shows the relationship between v_x and the vertical distance away from the interface (y) at $x = 100, 300, 500, 700$μm, confirming that the deformation is largely confined to the region close to the indenter face. Additionally, Fig. 6(b) indicates several aspects of the plastic boundary layer resulting from the interface friction between the material and the indenter face. Firstly, the velocity gradient, namely the boundary layer structure, differs depending on the value of the x-coordinate and a more pronounced velocity gradient is observed in the area closer to the indenter tip. As explained in Section 2.2, the friction stress along the indenter face increases linearly toward the indenter tip, suggesting that the boundary layer structure is determined by the friction condition at the interface. Specifically, the thickness of the plastic boundary layer increases near the indenter tip, where friction conditions are more severe. This observation is consistent with the findings of our previous study [11]. Secondary, velocity difference exists at the interface between the indenter and the material, namely, wall-slip occurs at the interface. In Fig. 6(b), v_{wall} is the velocity component of the indenter face in the x-direction, equivalent to $v_0\cos\alpha$ (v_0: indentation speed, α: half of indenter angle). As shown in this figure, the velocity of the material at the interface, i.e., $v_x(x,0)$, is lower than v_{wall}, which clearly shows the existence of the wall slip at the interface and causes the relative motion between the material and indenter at the interface shown in Fig. 5(b).

In order to quantitatively examine the relationship among interface friction, boundary layer structure, and wall-slip at the interface, wall-slip velocity $v_s(x)$ is defined as follows:

$$v_s(x) = v_{wall} - v_x(x,0) \tag{7}$$

Fig. 6(c) shows the distribution of $v_s(x)$ along the indenter face, indicating that $v_s(x)$ decreases toward the indenter tip. This decrease arises from material deformation at the interface caused by friction drag, where the velocity of the material $v_x(x,0)$ is higher near the indenter tip due to greater friction stress.

Furthermore, to examine the impact of wall-slip velocity on the boundary layer structure, the velocity field v_x (x,y), which is shown in Fig. 6(b), is normalized based on the following equation:

$$v_n(x,y) = \frac{v_x \quad (x,y)}{v_{wall} - v_s(x)} = \frac{v_x \quad (x,y)}{v_x \quad (x,0)} \tag{8}$$

Fig. 6(d) shows the normalized velocity field $v_n(x,y)$ at $x = 100, 300,$

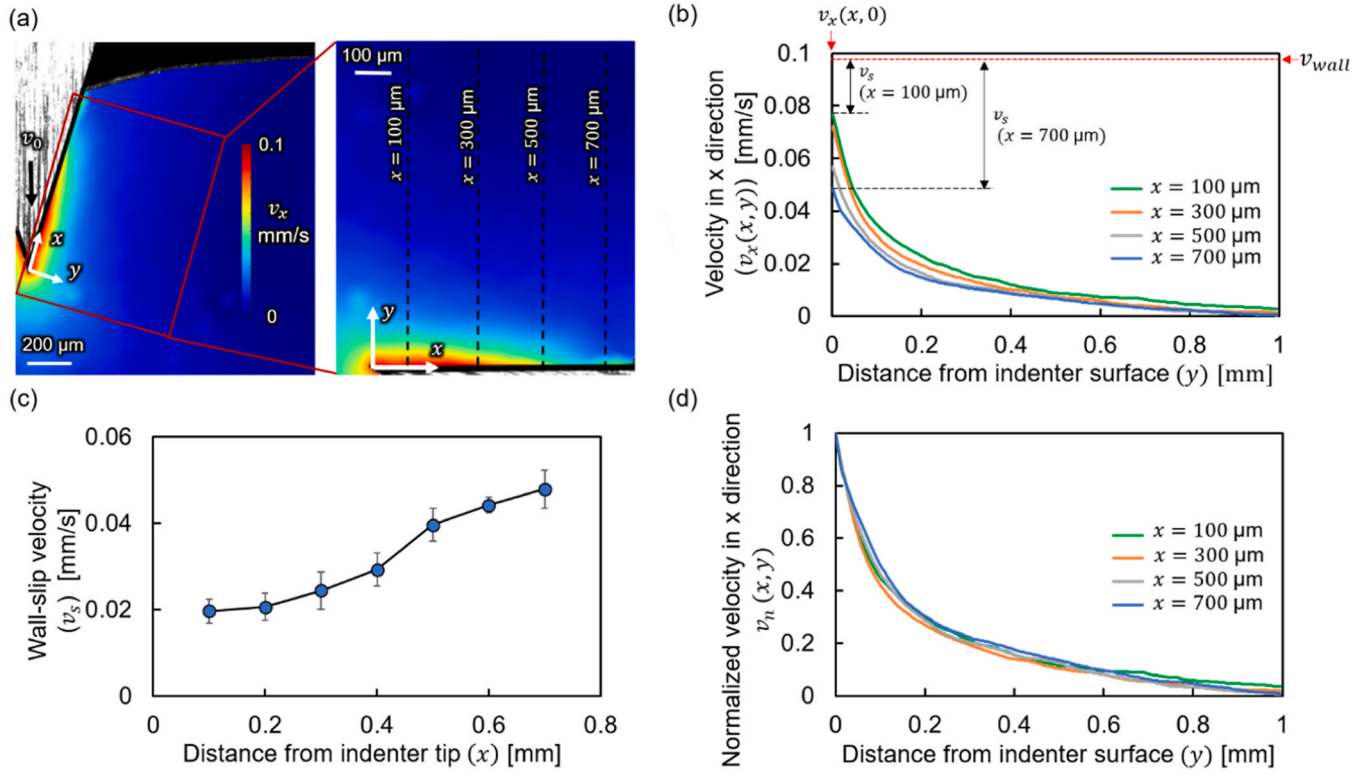

Fig. 6. (a) Velocity field of the x direction, (b) the relationship between v_x and y at different values of x axis, (c) wall-slip velocity distribution and (d) the relationship between v_n and y at different values of x axis ($x = 100, 300, 500, 700$μm).

500,700μm. In contrast to Fig. 6(b), all curves of the normalized velocity field nearly converge to a single curve, strongly suggesting that the boundary layer structure is determined by the wall-slip behavior at the interface. These findings suggest that the interface friction primarily determines the wall-slip behaviors at the interface, such as wall-slip velocity or wall-slip amount, which subsequently determines the bulk deformation of the material, i.e., the plastic boundary layer structure.

Note that the friction-induced plastic boundary layer is very similar to a laminar fluid boundary layer characterized by steep velocity gradients. However, a distinctive feature of the plastic boundary layer, overlooked in previous research [11,32], is the wall-slip behavior, which does not commonly occur in classical fluid mechanics' boundary layers. This distinction may be one of the features of the friction-induced plastic boundary layer, and aids in understanding friction-induced deformation behaviors, which are crucial for metal forming processes and tribology applications.

3.2. *The relationship between the wall-slip velocity and surface expansion distribution*

Explained in the preceding section, wall-slip behavior is pivotal in comprehending interface friction and its linked deformation patterns. Surface expansion stands out as a paramount phenomenon in sliding contact, exerting a significant influence on interface friction. Specifically, the surface expansion ratio—denoting the ratio between the original material's surface area and the area post-deformation—directly influences the exposure of chemically active nascent surfaces at the contact interface, which also directly corresponds to the adhesion force distribution at the interface. Additionally, the surface expansion ratio is distributed non-uniformly at the interface, and its distribution also changes as the friction condition at the interface during the deformation process. Prior research, including study [20], has paid limited attention to the factors influencing this distribution. Our study seeks to fill this gap by elucidating the relationship between surface expansion behavior and the wall-slip phenomenon, and identifying the key factors influencing the distribution of surface expansion at the sliding contact interface.

Fig. 7 depicts the procedure for obtaining distribution of surface expansion ratio $\phi(x,t)$ at any given time t. By tracking virtual markers placed at regular intervals of l on the metal surface (Fig. 7(a)) through PIV analysis, the position of tracking marker P_n from the indenter tip (x_n) and the distance between P_n and P_{n+1} ($l + \Delta l_{n\_n+1}$) at different time t during the indentation process can be obtained (Fig. 7(b)). The distance of midpoints x_{n_n+1} between P_n and P_{n+1} from the indenter tip, namely $x_{n\_n+1}(t)$ and the corresponding local surface expansion ratio $\phi_{n\_n+1}(t)$ at the position of point x_{n_n+1} at given time t are calculated by the following Eq. (9) and Eq. (10). The distribution of surface expansion ratio $\phi(x,t)$ is determined based on the local surface expansion ratio $\phi_{n\_n+1}(t)$ and local point $x_{n\_n+1}(t)$, respectively (Fig. 7(c)).

$$x_{n\_n+1}(t) = \begin{cases} 0 & (n=0) \\ \dfrac{x_n(t) + x_{n+1}(t)}{2} & (n>0) \end{cases} \tag{9}$$

$$\phi_{n\_n+1}(t) = \frac{\Delta l_{n\_n+1}(t)}{l} = \begin{cases} \dfrac{x_n(t) + x_{n+1}(t) - l}{l} & (n=0) \\ \dfrac{x_{n+1}(t) - x_n(t) - l}{l} & (n>0) \end{cases} \tag{10}$$

Fig. 8(a) shows images featuring superimposed virtual tracking markers (spacing $l = 25.6$ μm) at an indentation depth of 5 mm, demonstrating that the virtual tracking markers successfully visualize the local surface expansion along the indenter face. Note that, in Fig. 8 (a), the markers are highlighted every five points to clearly show the movement and positional relationship of each tracking marker. The tracking markers (P_1-P_5), initially placed on the metal surface at regular intervals (see Fig. 7(a)), demonstrate varied movement, reflecting different slip conditions along the interface face. Furthermore, Fig. 8(b) illustrates the surface expansion distribution $\phi(x,t)$ at specific time intervals—20, 30, 40, and 50 s—corresponding to indentation depths of

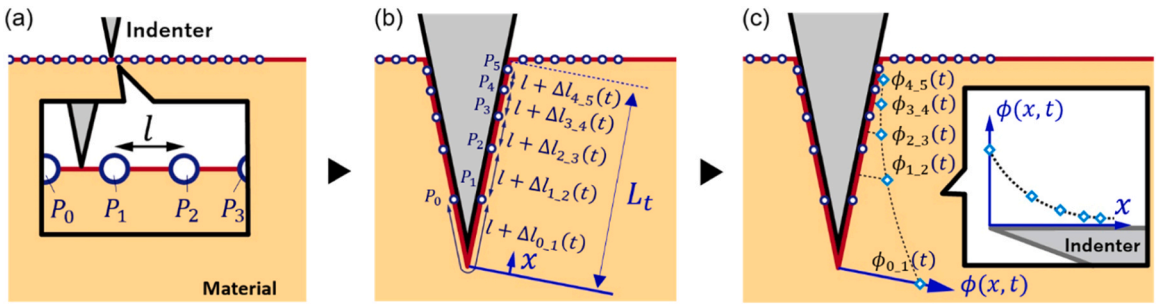

Fig. 7. The procedure for obtaining distribution of surface expansion ratio $\phi(x,t)$ at given time t.

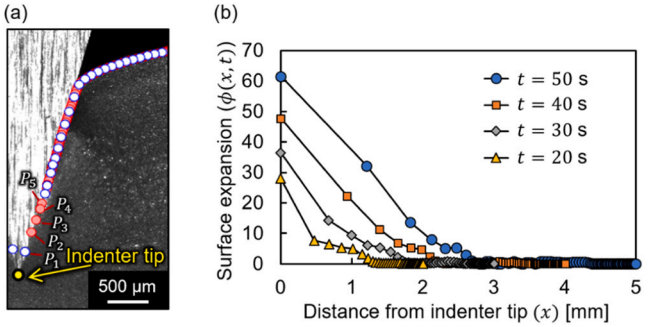

Fig. 8. Distribution of surface expansion ratio: (a) tracking markers with the depth of 5 mm and (b) surface expansion distribution at different given time t.

2.0, 3.0, 4.0, and 5.0 mm, respectively. Note that the surface expansion distribution $\phi(x,t)$ was obtained by averaging the data obtained from four experiments. As depicted in this figure, the surface expansion ratio varies along the indenter face, and the localization of the surface expansion in the vicinity of the indenter tip is evident. These results confirm the non-uniform nature of the surface expansion distribution along the indenter face and indicate that the localized surface expansion results in the severe frictional conditions near the indenter tip.

According to Eq. 10, the non-uniform surface expansion distribution is caused by the difference in the surface expansion deformation behavior at each two consecutive points along the indenter face at a given time. This uneven surface expansion distribution is closely linked to the wall-slip velocity at each point along the interface. To depict the relationship between surface expansion and wall-slip velocity, a schematic diagram in Fig. 9, illustrating the assumption of the movement of each tracking point under slip and no-slip conditions, is presented.

Assuming that the tracking points P_i ($i = 0, 1, 2, \ldots, n$) are plotted on the metal surface with the regular interval distance l before indentation (Fig. 9(a)) and $v_i(t)$ (wall-slip velocity) is the instantaneous velocity of the tracking marker P_i along the indenter face at a given time t. At any incremental time Δt, the corresponding wall-slip velocity for each two tracking markers P_n and P_{n+1} are $v_n(t+\Delta t)$ and $v_{n+1}(t+\Delta t)$.

The "macroscopic" surface expansion ratio over the entire deformation area can be defined as:

$$\phi = \frac{\Delta L}{L} = \frac{1-\sin\alpha}{\sin\alpha} \tag{11}$$

where ΔL represents the difference between the original surface length of the undeformed specimen, L, and the surface length after the indentation process (see Fig. 9(b)). Presuming that the contact condition at the interface adheres to a no-slip condition, i.e., the wall-slip does not occur at the indenter-material interface, where $v_i(t)$ equals to zero, the virtual tracking point at the metal surface moves integrally with the indenter (Fig. 9(c)), i.e., microscopic incremental length for each pair of two tracking markers, Δl, remains uniform, and the total Δl for all tracking markers is equal to ΔL. Under such conditions, the local microscopic surface expansion ratio $\phi_{n\_n+1}(t)$ for each pair of two tracking markers P_n and P_{n+1} at given time t could be expressed as:

$$\phi_{n\_n+1}(t) = \frac{\Delta l_{n\_n+1}(t)}{l} = \frac{\Delta l}{l} = \frac{1-\sin\alpha}{\sin\alpha} \tag{12}$$

This implies that in the absence of wall-slip at the interface, the surface expansion ratio remains consistently uniform across the entire contact area, maintaining the value consistent with the macroscopic surface expansion ratio. In other words, any difference in the surface expansion ratio should be attributed to the wall-slip behavior at the interface.

On the other hand, assuming that the contact condition at the interface follows the slip condition (Fig. 9(d)) —a scenario that more accurately reflects reality—, uneven friction condition at the interface inevitably results in different interface deformation behavior, causing changes in wall-slip velocity along the interface. According to Eq. 10, the

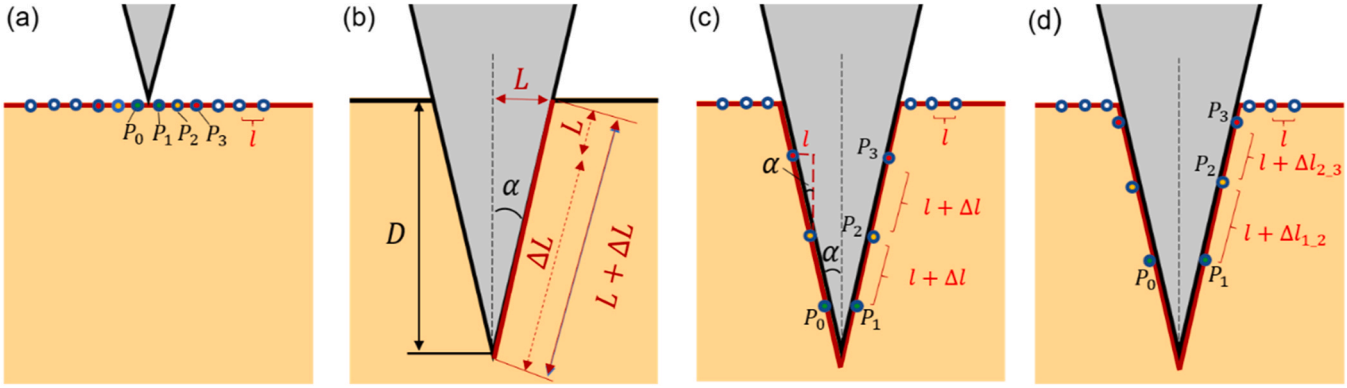

Fig. 9. Schematic of (a) initial distribution of tracking points before indentation, (b) macroscopic deformation after indentation, (c) distribution of tracking points under no-slip condition and (d) distribution of tracking points under slip condition after indentation.

incremental surface expansion ratio $\Delta\phi_{n\_n+1}(t)$ at any incremental time Δt for each two tracking markers P_n and P_{n+1}could be expressed as:

$$\Delta\phi_{n\_n+1}(t) = \phi_{n\_n+1}(t+\Delta t) - \phi_{n\_n+1}(t) = \frac{\Delta l_{n\_n+1}(t+\Delta t)}{l} - \frac{\Delta l_{n\_n+1}(t)}{l}$$
$$= \begin{cases} \dfrac{[x_0(t+\Delta t) - x_0(t)] + [x_1(t+\Delta t) - x_1(t)]}{l} = \dfrac{\int_t^{t+\Delta t}[v_0(t) + v_1(t)]dt}{l} & (n=0) \\ \dfrac{[x_{n+1}(t+\Delta t) - x_{n+1}(t)] - [x_n(t+\Delta t) - x_n(t)]}{l} = \dfrac{\int_t^{t+\Delta t}[v_{n+1}(t) - v_n(t)]dt}{l} & (n>0) \end{cases} \quad (13)$$

Here, $\phi_{n\_n+1}(t+\Delta t)$ and $\phi_{n\_n+1}(t)$ represent the microscopic surface expansion ratio for each two tracking markers P_n and P_{n+1} at given time $(t+\Delta t)$ and t, respectively. Meanwhile, $\Delta\phi_{n\_n+1}(t)$ is the incremental value of $\phi_{n\_n+1}(t)$ after an interval time of Δt. This suggests that the distribution of the surface expansion ratio should be determined by the distribution of the wall-slip velocity. To illustrate the wall-slip behavior at the indenter-material interface, the evolution of the distance from the indenter tip, x_n and wall-slip velocity, v_s, for each tracking point (P_1-P_5, see Fig. 8) are obtained through the PIV analysis, as shown in Fig. 10.

As shown in the Fig. 10, during the initial indentation, the tracking points are close to the indenter tip (Fig. 10 (a)), while exhibiting relatively high wall-slip velocity for each tracking point (Fig. 10 (b)). This occurrence is due to lower interface friction at the interface resulting from less fresh surface generated and smaller adhesion at the interface, manifesting as smaller incremental distance between consecutive points (Fig. 10 (a)). With the progress of indentation, the friction increases because of more nascent surface generated, thereby largely increasing the adhesion force at the interface, corresponding to large incremental distance of each two consecutive points (Fig. 10 (a)). Consequently, the wall-slip velocity for P_1 diminishes and remains nearly constant over time, even as the distance of P_1 extends far from the indenter tip. On the other hand, wall-slip velocity for tracking points P_2-P_5 decreases initially at small indentation depths but gradually increases over time (Fig. 10 (b)), leading to distinct growth trends in distance from the indenter tip (Fig. 10 (a)).

These differences in the deformation behaviors stem from strain hardening induced by intense plastic deformation near the indenter tip as the indentation depth increases. This phenomenon would hinder further deformation in the vicinity of indenter tip, causing a slowdown in the increasing distance of P_1 from the indenter tip (Fig. 10 (a)), as well as reflecting in an almost constant wall-slip velocity (Fig. 10 (b)). Subsequently, decreased deformability promotes surface deformation in regions farther from the indenter tip (Fig. 10 (a)), triggering an increase in wall-slip velocity for P_2-P_5 (Fig. 10 (b)). These findings distinctly illustrate the interrelation and mutual influence among interface friction, wall-slip velocity, and surface expansion distribution.

To verify the relationship between surface expansion distribution and wall-slip velocity, we compare the local surface expansion ratio $\phi_{n\_n+1}(t)$ of several two consecutive tracking markers with different given time t, calculated through the procedure for obtaining distribution of surface expansion ratio (see Eq.10), with the integral of wall-slip velocity $\phi_{n\_n+1}(t)_{calculated}$ (see Eq.13), as shown in Fig. 10. Note that Δt equals to 2 s in this figure. As demonstrated in Fig. 10, $\phi_{n_n+1}(t)$is highly consistent with $\phi_{n\_n+1}(t)_{calculated}$, indicating that the distribution of surface expansion ratio is indeed determined by that of the wall slip velocity. Fig. 11.

3.3. The influence of lubricants on surface expansion distribution

As discussed in the previous section, interface friction, wall-slip velocity, and surface expansion distribution are interconnected and mutually influential. Furthermore, the surface expansion distribution can serve as an indicator of friction force distribution at the contact

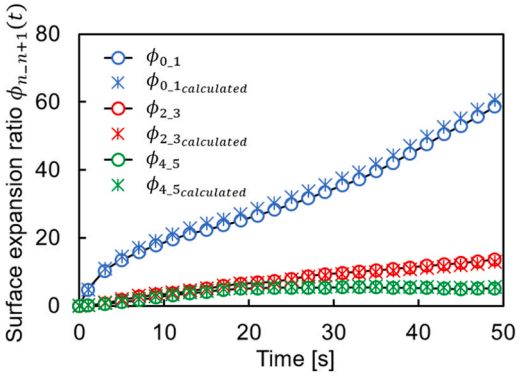

Fig. 11. The comparison between $\phi_{n_n+1}(t)$and $\phi_{n\_n+1}(t)_{calculated}$.

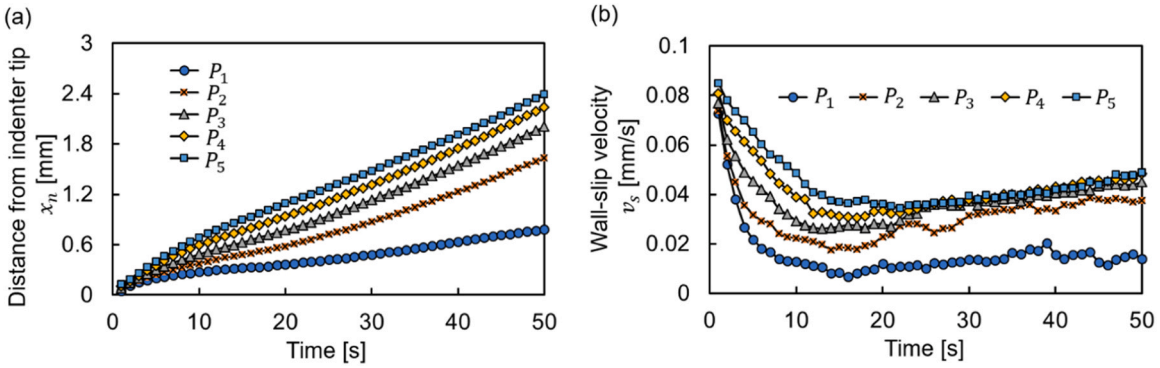

Fig. 10. (a) Distance from the indenter tip and (b) wall-slip velocity v_s for each tracking point over time.

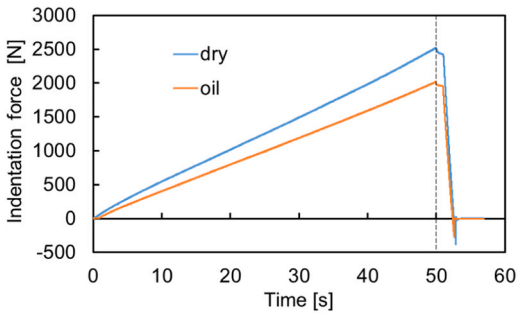

Fig. 12. The comparison of change in the indentation force with and without lubricant.

interface, potentially offering a quantitative means to assess the impact of lubricants in sliding contact scenarios.

Fig. 12 shows a comparison of the variation in indentation force over time at an indentation depth of 5 mm, conducted at a speed of 0.1 mm/s, both with and without the presence of a lubricant. A commercially available mineral-oil-based lubricant (refer to as 'oil') was employed in the lubricated condition [33]. The graph distinctly indicates that the indentation force under the lubricated condition is approximately 20% lower than that in the dry condition. This substantial reduction suggests an effective mitigation of interface friction due to the application of the lubricant. Moreover, Fig. 13 (a) and Fig. 13 (b) are the image of the 30 deg indenter, superimposed with the streaklines at $t = t_0 + 5$ s, with and without the lubricant. In these images, yellow and red points represent the endpoints of the streaklines and points on the indenter face tangent to the initial position of the endpoints, respectively. Additionally, Fig. 13 (c) presents a comparison of the slip amounts for each streakline (U_1-U_4) with and without the presence of oil. The results clearly show that the lubricant effectively increases the gap between the red and yellow points, representing the slip amount, at $t = t_0 + 5$ s, indicating the decreased interface friction at the interface. These findings are supported by observations of the indenter face after experiments

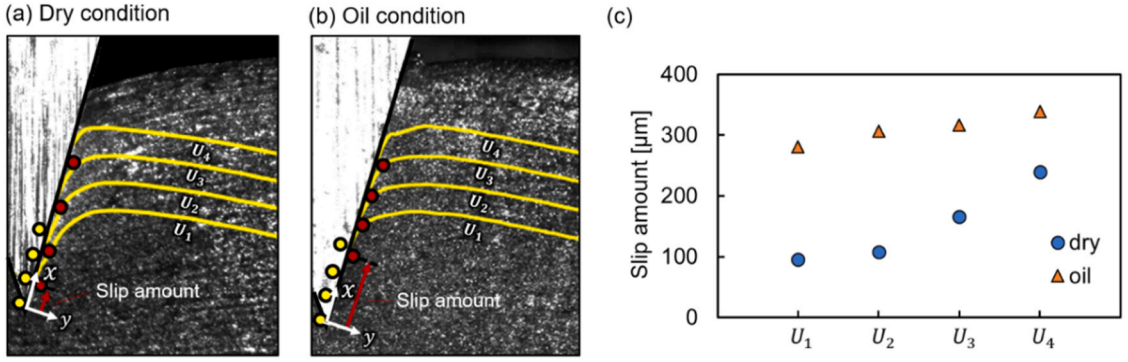

Fig. 13. The comparison of streaklines at $t = t_0 + 5$ s under (a) dry and (b) oil conditions and (c) slip amount for each streakline.

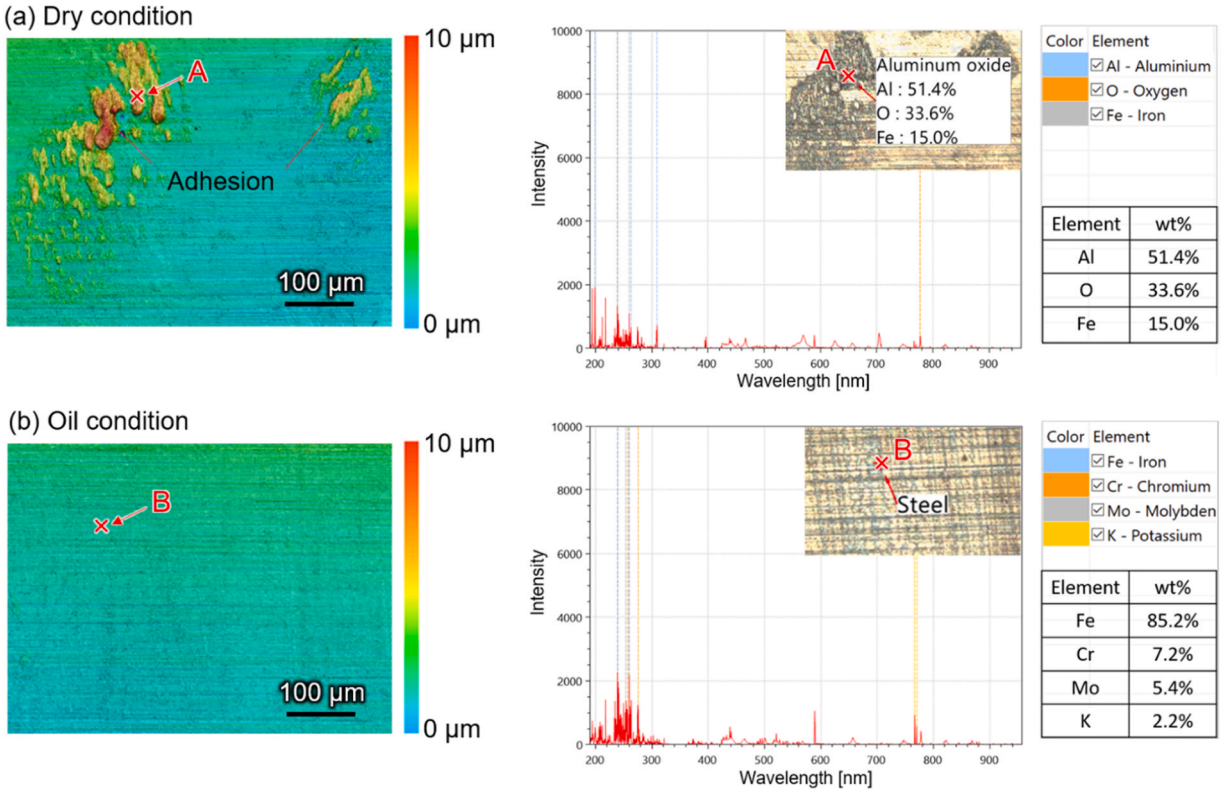

Fig. 14. Observation for indenter surface and its corresponding element analysis under (a) dry and (b) oil conditions.

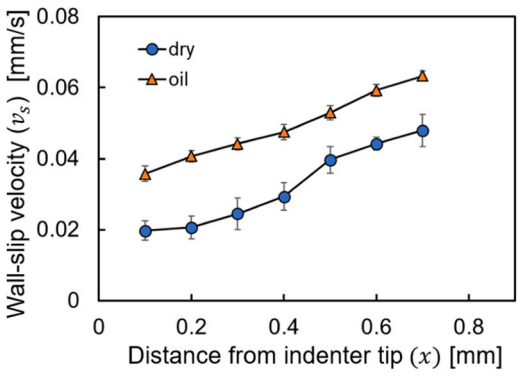

Fig. 15. The distribution of the wall slip velocity with and without lubricants.

(Fig. 14 (a) and (b)), and by the distribution of the wall slip velocity along the indenter face at $t = t_0 + 5$ s (Fig. 15), under both dry and lubricated conditions. Note that, in Fig. 14, the results of the element analysis at points A and B conducted using the Laser-Induced Breakdown Spectroscopy [34] are also presented. As shown in Fig. 14 (a) and (b), pronounced adhesion to the indenter face, identified as aluminum through the element analysis, is observed in a dry state (Fig. 14 (a)). In contrast, under the oil condition, minimal or no adhesion occurs (Fig. 14 (b)), indicating that the use of lubricant reduces interface friction. These variations in the state of interface friction manifest as differences in wall-slip behavior, with the wall-slip velocity under the lubricated condition being approximately 60% higher than that under dry conditions (Fig. 15), confirming the significant facilitation of sliding motion at the interface due to the presence of lubricant. These results decisively demonstrate the effective reduction of interface friction between the indenter and the material through the application of a mineral-oil-based lubricant.

Fig. 16 shows the images featuring superimposed virtual tracking markers at an indentation depth of 5 mm, with and without the application of lubricant, indicating alterations in the material's deformation behavior at the sliding contact attributable to the presence of lubricant. As seen in this figure, under the lubricated condition (Fig. 16 (b)), substantial wall-slip of the material results in pronounced surface expansion in the vicinity of the indenter tip. Fig. 17 provides a schematic diagram illustrating the impact of localization of the surface expansion at the indenter tip on the surface expansion distribution under the dry and lubricated conditions. When subjected to the same indentation depth in both dry and lubricated conditions, the total amount of surface expansion, ΔL, remains consistent (refer to Fig. 9(b)). As depicted in

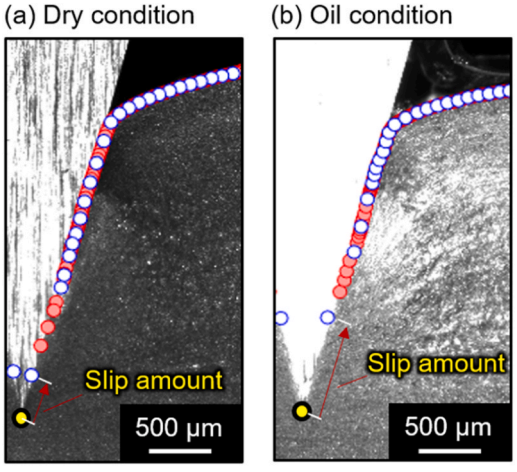

Fig. 16. Tracking markers under (a) dry and (b) oil conditions at the depth of 5 mm.

Fig. 17, at a given time interval Δt, the indenter initially contacts tracking points P_0 and P_1, resulting in corresponding wall-slip velocities v_0 and v_1. Due to the reduced interface friction in the presence of lubricant, v_0 and v_1 are greater than those under dry conditions. These larger values of v_0 and v_1 inevitably amplify the value of $\phi(0,t)$ (refer to Eq. 10 and Eq. 13), indicating that the surface expansion under lubricant conditions becomes more localized in the vicinity of indenter tip (Fig. 17 (b)). In other words, it should be possible to quantitatively visualize the lubricity at the interface by evaluating the degree of concentration of the distribution of the surface expansion ratio in the vicinity of the indenter tip.

To quantitatively show the influence of the lubricity on the surface expansion distribution, Fig. 18 (a) shows the distribution of the surface expansion distribution $\phi(x,t)$ at the indentation depth of 5 mm, namely at $t = 50$s, along the indenter face with and without lubrication. These results demonstrate a significant increase of almost 76% in the surface expansion ratio near the indenter tip due to the effect of the lubricant, confirming that variations in frictional conditions at the interface affect the distribution of the surface expansion ratio. This insight also introduces a method for quantitative evaluation, moving beyond traditional qualitative assessments, which commonly employs FEM analysis to estimate surface expansion ratio or friction tests to evaluate lubricant performances [19,35].

Moreover, Fig. 18 (b) compares the normalized surface expansion ratio distribution, $\phi_n(x,t)$, was defined as the following equation, with and without the presence of the lubricant.

$$\phi_n(x,t) = \frac{\phi(x,t)}{\phi(0,t)} \tag{14}$$

This figure further demonstrates that the surface expansion distribution under the oil condition becomes more localized and less diffused compared to that under the dry condition. In other words, oil lubricants reduce interface friction, enabling increased wall-slip velocity between the indenter and material at the interface in the vicinity of the indenter tip. This, in turn, triggers pronounced localized surface expansion. To put it simply, more localized surface expansion ratio in the vicinity of indenter tip compared to that under dry condition, indicates a higher wall-slip velocity at the interface, which reflects smaller interfacial friction.

Based on the discussion above, it may be possible to assess lubricating efficiency of lubricants at the severe sliding contact quantitatively, by evaluating the deformation behavior of the material at the material-indenter interface. The reduction in interface friction attributed to lubricants promotes an escalation in wall-slip velocity, inducing highly localized surface expansion near the indenter edge. The characterization of surface expansion distribution, coupled with its correlation to wall-slip velocity, serves as an effective quantitative assessment of lubricating effectiveness.

4. Conclusion

Interface friction is fundamental to tribology, which has considerable impact on the interface phenomena in machining and forming processing. This work focuses on the relationship between interface friction and plastic boundary layer phenomenon, as well as surface expansion distribution, by using high-speed imaging and particle image velocimetry techniques. The key findings and conclusions are summarized as followed:

(1) Assuming that the maximum indentation force reflects the frictional force between the indenter and the material, the friction stress along the side face of the indenter increases linearly toward the indenter tip.
(2) The friction-induced plastic deformation flow observed in the vicinity of the severe sliding contact is very similar to a laminar

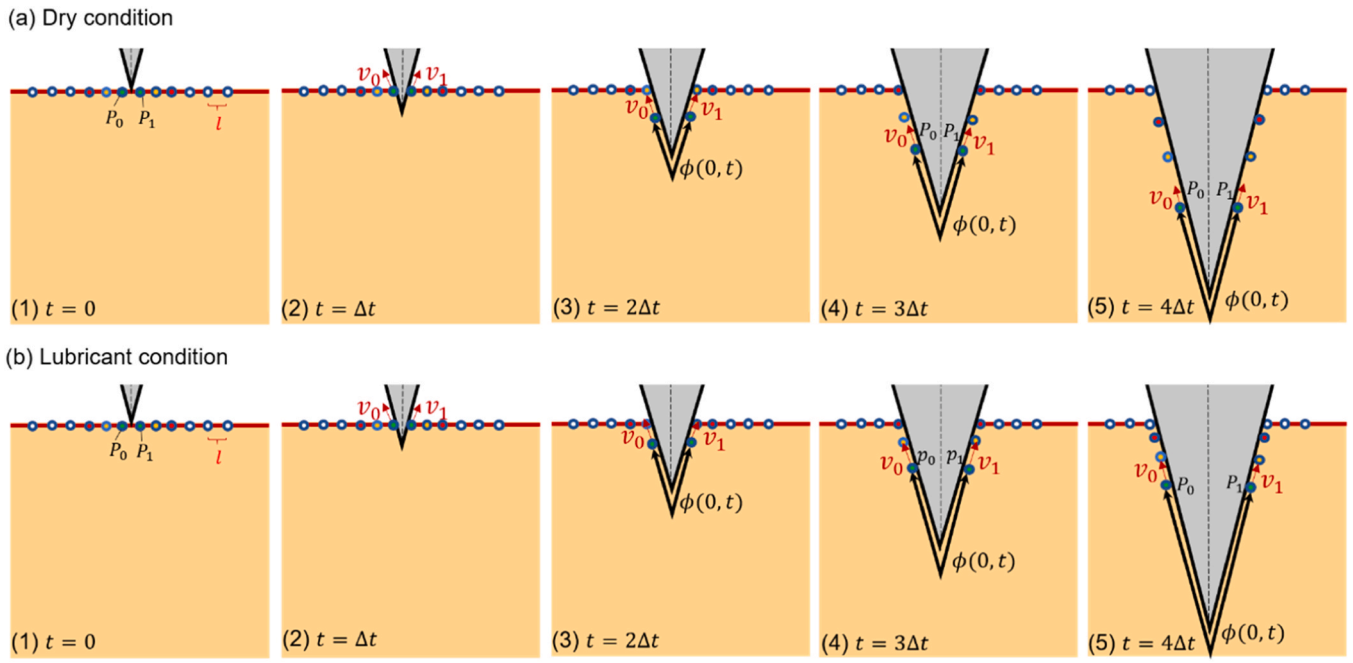

Fig. 17. The schematic diagram of the influence of wall-slip velocity on surface expansion distribution under (a) dry and (b) lubricant conditions.

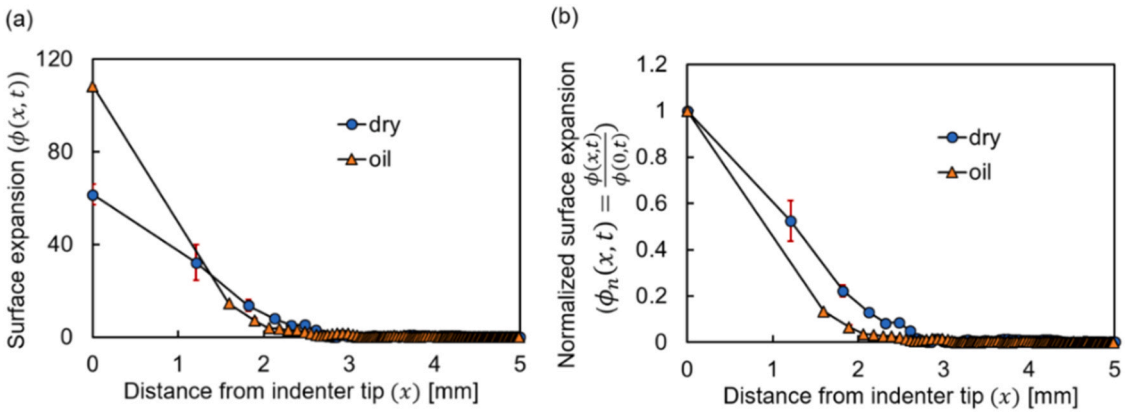

Fig. 18. The comparison of (a) surface expansion distribution $\phi(x,t)$ and (b) normalized surface expansion ratio distribution $\phi_n(x,t)$ with and without lubricants at the given time t of 50 s.

fluid boundary layer, albeit distinct due to the presence of wall-slip velocity.

(3) The interface friction primarily determines the wall-slip behaviors at the interface, which subsequently determines the bulk deformation of the material, i.e., the plastic boundary layer structure.

(4) Non-uniform surface expansion distribution results from the difference in the wall-slip velocity along the sliding surface caused by the interface friction. Since the surface expansion distribution also determines the degree of the exposure of freshly generated nascent surface and subsequently influences interface friction, it can be said that interface friction, wall-slip velocity, and surface expansion distribution interact with each other.

(5) Our observation demonstrates that the application of lubricant greatly influences the deformation behavior at the contact interface and alters the wall-slip velocity and localized surface expansion by 60% and 76%, respectively. Therefore, it may be possible to assess lubricating efficiency of lubricants at the sliding contact quantitatively, by evaluating the deformation behavior of the material at the material-indenter interface.

Funding sources

This work was supported by JSPS KAKENHI Grant Number 22H01376 and 22K18758, Amada Foundation Grant Number AF-2019038-C2, and Machine Tool Engineering Foundation RU-18.

CRediT authorship contribution statement

Tatsuya Sugihara: Writing – review & editing, Visualization, Supervision, Project administration, Methodology, Funding acquisition, Conceptualization. **Toshiyuki Enomoto:** Writing – review & editing, Resources. **Xiaoke Lin:** Writing – original draft, Software, Methodology, Investigation, Data curation, Conceptualization.

Declaration of Competing Interest

The authors declare the following financial interests/personal relationships which may be considered as potential competing interests: Tatsuya Sugihara reports financial support was provided by Japan Society for the Promotion of Science. Tatsuya Sugihara reports financial

support was provided by Amada Foundation. Tatsuya Sugihara reports financial support was provided by Machine Tool Engineering Foundation. If there are other authors, they declare that they have no known competing financial interests or personal relationships that could have appeared to influence the work reported in this paper.

Data availability

Data will be made available on request.

Acknowledgements

We would like to acknowledge Professor Srinivasan Chandrasekar (Purdue University) for discussions on the manuscript. We thank everyone at L.P.S. Works Co., Ltd., and Neos Co., Ltd., for their invaluable assistance.

Statement of Originality

As the corresponding author I certify that this manuscript is original and its publication does not infringe any copyright. As the corresponding author I declare that the manuscript has not been previously published, in whole or in part in any other journal or scientific publishing company. Also, the manuscript does not participate in any other publishing process. I also declare there is no conflict of interest.

As the corresponding author I declare that all persons listed hereafter were committed in the creation of the paper and were informed about their participation.

References

[1] Lin SY. Analysis of the dissimilar interface frictional constraints during the upsetting process. Int J Adv Manuf Technol 1997;13(9):601–10. https://doi.org/10.1007/bf01350818.
[2] Menezes Pradeep L, Kumar K, Kishore, Kailas Satish V. Influence of friction during forming processes—a study using a numerical simulation technique. Int J Adv Manuf Technol 2009;40(11-12):1067–76. https://doi.org/10.1007/s00170-008-1425-5.
[3] Lupoi R, Osman FH. Under surface pressure sensing technique for the evaluation of contact stresses. J Mater Process Technol 2005;164-165:1537–43. https://doi.org/10.1016/j.jmatprotec.2005.02.022.
[4] Hua-Chu Shih, Wilson William RD. Effects of contact pressure and strain on friction in sheet-metal forming©. Tribology Trans 1999;42(1):144–51. https://doi.org/10.1080/10402009908982201.
[5] Saha Pradip K, Wilson William RD. Influence of plastic strain on friction in sheet metal forming. Wear 1994;172(2):167–73. https://doi.org/10.1016/0043-1648(94)90284-4.
[6] Wang SL, Rao KP. An upper-bound analysis of friction in metal forming. Int J Mech Sci 1997;39(2):201–9. https://doi.org/10.1016/0020-7403(96)00054-9.
[7] Hsu Tze-Chi, Huang Chien-Chin. The friction modeling of different tribological interfaces in extrusion process. J Mater Process Technol 2003;140(1-3):49–53. https://doi.org/10.1016/s0924-0136(03)00724-6.
[8] Rigney DA, Hirth JP. Plastic deformation and sliding friction of metals. Wear 1979;53(2):345–70. https://doi.org/10.1016/0043-1648(79)90087-5.
[9] Rigney DA. Transfer, mixing and associated chemical and mechanical processes during the sliding of ductile materials. Wear 2000;245(1-2):1–9. https://doi.org/10.1016/s0043-1648(00)00460-9.
[10] Viswanathan Koushik, Udupa Anirudh, Yeung Ho, Sagapuram Dinakar, Mann James B, Saei Mojib, Chandrasekar Srinivasan. On the stability of plastic flow in cutting of metals. CIRP Ann - Manuf Technol 2017;66(1):69–72. https://doi.org/10.1016/j.cirp.2017.04.027.
[11] Sugihara Tatsuya, Udupa Anirudh, Viswanathan Koushik. A plastic boundary layer in wedge indentation of aluminum. Mater Trans 2019;60(8):1436–41. https://doi.org/10.2320/matertrans.MD201907.
[12] Udupa Anirudh, Sundaram Narayan, Sugihara Tatsuya, Chandrasekar Srinivasan. Direct In Situ observation of deformation modes in wedge indentation of metals. Mater Trans 2019;60(8):1442–9. https://doi.org/10.2320/matertrans.MD201906.
[13] Bourgin Patrick. Fluid-film flows of differential fluids of complexity n dimensional approach—applications to lubrication theory. J Lubr Technol 1979;101(2):140–4. https://doi.org/10.1115/1.3453294.
[14] Cross Benjamin, Barraud Chloé, Picard Cyril, Léger Liliane, Restagno Frédéric, Charlaix Élisabeth. Wall slip of complex fluids: Interfacial friction versus slip length. Phys Rev Fluids 2018;3(6):1–9. https://doi.org/10.1103/PhysRevFluids.3.062001.
[15] Noh Jeong Hoon, Hwang Beong Bok. Influence of punch geometry on surface deformation and tribological conditions in backward extrusion. J Mech Sci Technol 2018;32(1):323–31. https://doi.org/10.1007/s12206-017-1232-8.
[16] Duran Deniz, Özdemir Izzet. Predicting and measuring surface enlargement in forward rod extrusion. J Manuf Sci Eng 2016;138(7):1–7. https://doi.org/10.1115/1.4032261.
[17] Noh Jeong-hoon, Hwang Beong Bok, Lee Ho Yong. Influence of punch face angle and reduction on flow mode in backward and combined radial backward extrusion process. Met Mater Int 2015;21(6):1091–100. https://doi.org/10.1007/s12540-015-5276-y.
[18] Ok JH, Hwang Beong Bok. An analysis on the surface expansion of aluminium alloys in backward can extrusion process. Mater Sci Forum 2006;519-521:931–6. https://doi.org/10.4028/www.scientific.net/MSF.519-521.931.
[19] Sagisaka Yoshihiro, Nakamura Tamotsu, Hayakawa Kunio, Ishibashi Itaru. Evaluation of environmentally friendly lubricant for aluminum cold forging using friction test based on spline extrusion. J Manuf Process 2013;15(1):96–101. https://doi.org/10.1016/j.jmapro.2012.09.006.
[20] Lin Xiaoke, Kinoshita Seiji, Sugihara Tatsuya, Enomoto Toshiyuki. Exploring the role of the interface adhesion phenomena focusing on surface expansion distribution. 108160 Tribology Int 2023;Volume 179:1–8. https://doi.org/10.1016/j.triboint.2022.108160.
[21] Arsecularatne JA. On tool-chip interface stress distributions, ploughing force and size effect in machining. Int J Mach Tools Manuf 1997;37(7):885–99. https://doi.org/10.1016/s0890-6955(97)00001-1.
[22] Laakso Sampsa VA, Bushlya Volodymyr, Ståhl Jan-Eric. The correct way of splitting tools – optimization of instrument design for measuring contact stress distribution. Procedia Manuf 2018;25:97–102. https://doi.org/10.1016/j.promfg.2018.06.062.
[23] Guo Y, Compton WD, Chandrasekar S. In situ analysis of flow dynamics and deformation fields in cutting and sliding of metals. 20150194 Proc R Soc A: Math, Phys Eng Sci 2015;471(2178):1–18. https://doi.org/10.1098/rspa.2015.0194.
[24] Mahato Anirban, Yeung Ho, Guo Yang, Viswanathan Koushik, Sundaram Narayan K, Udupa Anirudh, Mann James B, Chandrasekar Srinivasan. Sinuous flow and folding in metals: implications for delamination wear and surface phenomena in sliding and cutting. Wear 2017;376-377:1534–41. https://doi.org/10.1016/j.wear.2017.02.012.
[25] Udupa Anirudh, Sugihara Tatsuya, Viswanathan Koushik, Chandrasekar Srinivasan. Altering the stability of surface plastic flow via mechanochemical effects. 014021 Phys Rev Appl 2019;11(1):1–16. https://doi.org/10.1103/PhysRevApplied.11.014021.
[26] Sugihara Tatsuya, Udupa Anirudh, Viswanathan Koushik, Davis Jason M, Chandrasekar Srinivasan. Organic monolayers disrupt plastic flow in metals. eabc8900 Sci Adv 2020;6(51):1–7. https://doi.org/10.1126/sciadv.abc8900.
[27] Groche P, Resch F. Dry forming of aluminum alloys - wear mechanisms and influencing factors. Mater und Werkst 2015;46(8):813–28. https://doi.org/10.1002/mawe.201500429.
[28] Kim W, Kawai K, Koyama H. Metal flow in wedge indentation of V- and W-shaped tools. J Mater Process Technol 2007;189(1-3):392–400. https://doi.org/10.1016/j.jmatprotec.2007.02.011.
[29] Gnanamanickam Ebenezer P, Lee Seongeyl, Sullivan John P, Chandrasekar Srinivasan. Direct measurement of large-strain deformation fields by particle tracking. 095710 Meas Sci Technol 2009;20(9):1–12. https://doi.org/10.1088/0957-0233/20/9/095710.
[30] Enomoto Toshiyuki, Sugihara Tatsuya, Yukinaga Satoshi, Hirose Kenji, Satake Urara. Highly wear-resistant cutting tools with textured surfaces in steel cutting. CIRP Ann 2012;61(1):571–4. https://doi.org/10.1016/j.cirp.2012.03.123.
[31] Pirozzoli Sergio. Revisiting the mixing-length hypothesis in the outer part of turbulent wall layers: mean flow and wall friction. J Fluid Mech 2014;745:378–97. https://doi.org/10.1017/jfm.2014.101.
[32] Wright PK, Horne JG, Tabor D. Boundary conditions at the chip-tool interface in machining: comparisons between seizure and sliding friction. Wear 1979;54(2):371–90. https://doi.org/10.1016/0043-1648(79)90128-5.
[33] Schmid SR, Saha PK, Wang J, Schmitz T. Developments in tribology of manufacturing processes. J Manuf Sci Eng 2020;142(11):1–11. https://doi.org/10.1115/1.4047723.
[34] Cremers David A, Chinni Rosemarie C. Laser-induced breakdown spectroscopy—capabilities and limitations. Appl Spectrosc Rev 2009;44(6):457–506. https://doi.org/10.1080/05704920903058755.
[35] Zareh-Desari Behrooz, Davoodi Behnam. Assessing the lubrication performance of vegetable oil-based nano-lubricants for environmentally conscious metal forming processes. J Clean Prod 2016;135:1198–209. https://doi.org/10.1016/j.jclepro.2016.07.040.